PERGAMON

Journal of Structural Geology 23 (2001) 1491–1505

JOURNAL OF STRUCTURAL GEOLOGY

www.elsevier.com/locate/jstrugeo

Solution-mass-transfer deformation adjacent to the Glarus Thrust, with implications for the tectonic evolution of the Alpine wedge in eastern Switzerland

Uwe Ring[a,*], Mark T. Brandon[b], Alexander Ramthun[a]

[a]*Institut für Geowissenschaften, Johannes Gutenberg-Universität, Becherweg 21, 55099 Mainz, Germany*
[b]*Department of Geology and Geophysics, Yale University, 210 Whitney Avenue, New Haven, CT 06520, USA*

Received 26 April 2000; revised 15 January 2001; accepted 25 January 2001

Abstract

We have studied aspects of absolute finite strain of sandstones and the deformation history above and below the Glarus Thrust in eastern Switzerland. The dominant deformation mechanism is solution mass transfer (SMT), which resulted in the formation of a semi-penetrative cleavage. Our analysis indicates that the Verrucano and Melser sandstones, which lie above the thrust, were deformed coaxially, with pronounced contraction in a subvertical Z direction and minor extension in a subhorizontal X direction, trending at ~200°. Most of the contraction in Z was balanced by mass-loss volume strains, averaging ~36%. Below the Glarus Thrust, sandstones of the North Helvetic flysch have smaller principal strains but similar volume strains. Deformation there was also approximately coaxial. The X direction is horizontal and trends ~160°, which is different by ~40° from the X direction in the hanging wall. The hanging wall of the Glarus Thrust (Verrucano and Melser sandstones) was deformed first, after it was accreted deep beneath the Alpine wedge. Continued northward advance of the wedge, accomplished in part by motion on the Glarus Thrust, allowed the wedge to override and accrete the North Helvetic flysch, which then started to form an SMT cleavage. The difference in X directions may reflect a change in transport direction, but this conclusion is difficult to accept since extension was minor and was accommodated by coaxial flattening, and not simple shear. Our work indicates that mass-loss volume strains were important in sandstones of the Helvetic nappes. The missing mass cannot be accounted for at the local scale, and appears to have been transported beyond the Helvetic zone. © 2001 Published by Elsevier Science Ltd.

1. Introduction

The Glarus Thrust is the sole thrust of the Helvetic nappes and a conspicuous feature in the landscape of the Glarus Alps (Fig. 1). In 1841, Arnold Escher von der Linth discovered the Glarus Thrust, but was reluctant to publish his observations: "No one would believe me, they would put me into an asylum" (p. 195 in Greene, 1982). Further work by Marcel Bertrand (1884), Edward Suess (1904, 1909), and Albert Heim (1919) established the geometry and origin of this impressive structure. Bertrand's publication in 1884 is widely regarded as marking the birth of the Alpine nappe theory (Trümpy, 1998), with the Glarus Thrust recognised as the type example of an orogen-scale thrust fault.

The Glarus Thrust separates the Infrahelvetic complex in its footwall from the Helvetic nappes in its hanging wall. Both units were derived from the Helvetic zone, which refers to the Mesozoic passive margin that bordered the southern side of the European continent. The underlying Infrahelvetic complex is distinguished by a thick sequence of syn-orogenic turbidites, and underlying Mesozoic platform carbonates of the European margin. The turbidites are locally volcanoclastic (e.g. Taveyannaz sandstone). Sinclair (1992) compared the Eocene and Oligocene turbidites of the Infrahelvetics with trench-fill turbidites formed at ocean–continent subduction zones. An important distinction is that both the Infrahelvetics and Helvetics were originally underlain by European continental crust, and not by oceanic crust.

The Glarus Thrust itself is marked by a <1-m-thick layer of highly sheared calc-mylonite (Lochseitenkalk) (e.g. Hsü, 1969; Trümpy, 1969; Schmid, 1975), which separates Eocene–Oligocene turbidites below the thrust from conglomerate and mudstone of the Permian Verrucano Formation above (Heim, 1919; fig. 33 in Trümpy, 1980). The Lochseitenkalk itself probably derived from Jurassic limestone (Schmid, 1975) and was carried up and over the footwall of the Glarus Thrust. Ductile shearing was certainly important during nappe transport, but significant brittle slip must have occurred as well. The reason is that the

* Corresponding author. Fax: +49-6131-3922164.
E-mail address: ring@mail.uni-mainz.de (U. Ring).

0191-8141/01/$ - see front matter © 2001 Published by Elsevier Science Ltd.
PII: S0191-8141(01)00015-3

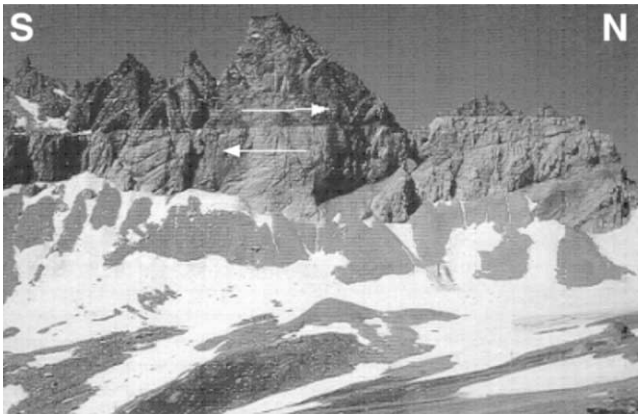

Fig. 1. The Glarus Thrust WSW of Elm.

break beneath the Lochseitenkalk marks a major stratigraphic discontinuity, with Jurassic limestone and Permian Verrucano overlying Eocene North Helvetic flysch. Thus, localised slip is needed to account for the observed stratigraphic offset.

The Glarus Thrust is folded into a broad, east–west trending antiform with gently dipping limbs (Schmid, 1975). Geologic estimates require >50 km of offset on the Glarus Thrust (Milnes and Pfiffner, 1980). Models addressing the mechanics of the Glarus Thrust have been proposed by Hsü (1969) and Schmid (1975). Milnes and Pfiffner (1977), Pfiffner (1981), Sinclair (1992) and Lihou (1996), amongst others, discussed the tectonic evolution of the Helvetic nappes and the Infrahelvetic complex of eastern Switzerland.

We focus here on the deformation history below and above the Glarus Thrust, and how deformation within the adjacent nappes relates to offset on the Glarus Thrust. Siddans (1979) studied relative strain in Permian mudstones of the Verrucano Formation, which lies above the Glarus Thrust in the Glarus nappe. His R_f/ϕ analysis on reduction spots showed a slightly prolate strain symmetry. These data lack information about volume strain, which is needed to estimate the strain type (i.e. constrictional, plane strain or flattening; Ramsay and Wood, 1973; Brandon, 1995).

Feehan and Brandon (1999) and Ring and Brandon (1999) reported new methods (PDS, Mode and SMT-fibre methods), which allow measurement of absolute strains and internal rotation in low-grade sandstone deformed by the solution-mass-transfer (SMT) mechanism (i.e. pressure solution). The application of those methods to sandstone from subduction-related accretionary wedges along the western North American margin indicates considerable mass-loss volume strains, on the order of 30–40% (Feehan and Brandon, 1999; Ring and Brandon, 1999). The volume loss is attributed to dissolution and bulk removal of the more soluble components of the rock by regional-scale fluid flow during SMT deformation.

The SMT mechanism is thought to be a linear viscous deformation mechanism, which operates by selective dissolution, transport, and precipitation along grain boundaries. What remains poorly understood is how these grain-boundary processes operate and interact, and what processes control the rate of SMT deformation in nature. The 'wet' Coble creep model (Elliott, 1973; Rutter, 1983) considers diffusional transport along grain boundaries to be the rate-limiting step. However, the finding that SMT deformation in accretionary wedges is commonly associated with considerable volume loss suggests that dissolution, precipitation, or advective fluid transport could be the rate controlling processes (Raj and Chyung, 1981; Mullis, 1993; Paterson, 1995).

Our study here was motivated by an interest in comparing deformation of siliciclastic rocks in a typical foreland fold-and-thrust belt with our results from subduction settings. We might expect some similarities given that deformation in both settings occurred in actively accreting convergent wedges. We knew in advance that SMT was the dominant deformation mechanism in siliciclastic rocks of the Glarus Alps, based on previous fabric work (Schmid, 1975; Siddans, 1979) and estimates of maximum temperature (100–350°C, Burkhard et al., 1992; Rahn et al., 1994, 1995, 1997). In this paper, we report the first absolute finite-strain data from the Glarus Alps. These data are used to evaluate the role of SMT deformation and volume strains in the tectonic evolution of the Glarus Thrust.

2. Overview

2.1. Geologic and tectonic setting

Tectonic units in the Alps are commonly named after the paleogeographic zones from whence they were derived. The Pennine zone represents a largely oceanic unit that separated the European margin from the Adriatic microcontinent, the latter of which is now represented by the Austroalpine nappes (e.g. Trümpy, 1980). The Helvetic zone describes those rocks associated with the Mesozoic passive margin that flanked the southern edge of the European plate. Alpine orogenesis in the Helvetic zone started in the Late Eocene (Pfiffner, 1986) when this margin was overridden by the Pennine and the Austroalpine nappes, with the North Penninic Prättigau flysch being the first to be obducted onto the margin. This event is generally considered to mark the final closure of oceanic basins in the Alps and the onset of full continental collision between the European and Adriatic continental margins. Thrusting propagated northward, progressing from the more internal nappes in the south to the more external foreland units in the north (Trümpy, 1969; Milnes and Pfiffner, 1977; Pfiffner, 1986). Structural burial is recorded by metamorphism at about 30–35 Ma (Hunziker et al., 1986), locally culminating in amphibolite-facies conditions in the southern parts of the Gotthard Massif (Frey et al., 1974). In the southern Helvetic nappes, metamorphism locally reached greenschist facies and was largely coeval with the major phase of nappe stacking and associated cleavage formation (D_2 or Calanda phase of Milnes and Pfiffner, 1977).

The Helvetic nappes above the Glarus Thrust can be subdivided in ascending order into the Glarus, Mürtschen, Axen and Säntis nappes (Figs. 2 and 3). The only pre-Mesozoic unit in the Helvetic nappes is the Permian Verrucano Formation, which makes up the lower two thirds of the Glarus nappe. In the Glarus Alps, metamorphism of the Verrucano reached anchizonal to incipient epizonal conditions (illite crystallinity; Siddans, 1979; Frey, 1988) with peak temperatures of 300–350°C in the area immediately above the southernmost part of the Glarus Thrust. Metamorphic grade decreases to the north, in the direction of decreasing structural depth.

The Infrahelvetic complex describes a structural assembly of Helvetic zone rocks that now lie beneath the Glarus Thrust. It is made up of four tectonic units, which are, in ascending structural order (Figs. 2 and 3):

1. the Aar Massif with its autochthonous and parautochthonous cover;
2. the Eocene to Oligocene North Helvetic flysch, which was, at least in part, stripped off the Mesozoic cover of the Aar Massif (Schmid, 1975);
3. the Blattengrat (South Helvetic) and Sardona (Ultrahelvetic or Penninic) nappes, which root much farther to the south relative to the Helvetic nappes (Trümpy, 1969; Schmid, 1975; Milnes and Pfiffner, 1977; Lihou, 1996); and
4. the so-called Subhelvetic nappes (consisting of Mesozoic cover stripped from the Aar Massif), which were also transported northwards before the Glarus Thrust formed (Schmid, 1975).

Metamorphism in the Infrahelvetic complex probably occurred at 20–25 Ma (Hunziker et al., 1986), and reached 270–300°C and 2–3 kbar in the southernmost part and 170–190°C and 1.3–1.5 kbar farther north (Rahn et al., 1994, 1995).

2.2. Deformation history

Lihou (1996) showed that the North Penninic Prättigau flysch, the Sardona nappe, and the South Helvetic Blattengrat nappe were juxtaposed and imbricated during an early deformational event, the D_1 or Pizol phase of Milnes and Pfiffner (1977). The Eocene to Lower Oligocene North Helvetic flysch, including the Taveyannaz sandstone, was deposited in front of the advancing Pizol-phase thrust wedge (Sinclair, 1992). The inferred tectonic transport direction during the Pizol phase, as deduced from calcite and quartz fibre lineations, was top-side towards ~340° (Lihou, 1996). Lihou (1996) estimated that this event started in Bartonian to Priabonian time (~40 Ma). According to Pfiffner (1978), the Sardona and Blattengrat nappes originated more than 30 km south of their present position. These nappes, together with all of the Helvetic nappes, were derived from the south-facing carbonate margin that flanked the southern edge of the European continent during the Mesozoic. This relationship indicates that parts of the Infrahelvetic units (i.e. the Blattengrat and Sardona nappes) were transported over the Helvetic domain during their collision with the European margin. Note that younger motion on the Glarus Thrust allowed the originally more inboard Helvetic nappes to override the Blattengrat and Sardona nappes (Milnes and Pfiffner, 1977), which is the configuration we observe today. Thus, the motion on the Glarus Thrust is 'back-stepping' or 'out-of-sequence', since it cuts across previously accreted nappes. We return to this point below.

Rocks of the Helvetic nappes were originally deposited on basement located between the Aar and Gotthard Massifs and on the Gotthard Massif. They were emplaced during the D_2 or Calanda phase of Milnes and Pfiffner (1977). Internal imbrication of the Helvetic nappes was closely followed by peak metamorphism in the Early Oligocene (30–35 Ma) (Frey et al., 1973; Hunziker et al., 1986).

Thrust faults in convergent wedges typically chop their way forward towards the foreland, which results in the accretion of imbricate slices from the downgoing plate. Such behaviour is called 'in-sequence' or perhaps more precisely, 'forward-stepping'. 'Out-of-sequence' or 'back-stepping' faults occur when a new imbricate fault splays off a deep part of the basal thrust and cuts up through the overlying thrust wedge. The result is that the front of the wedge becomes dismembered and overridden by the rear of the wedge. In some cases, the frontal pieces of the wedge are found re-accreted to the base of the wedge.

Paleogeography and structural relationships described above show that the Glarus Thrust is a back-stepping thrust, which means that the Infrahelvetic complex represents a slice that was originally accreted at the front of the wedge, prior to formation of the Glarus Thrust. Schmid (1975) argued that the S_2 Calanda-phase cleavage in the Verrucano formed before motion on the Glarus Thrust was initiated. Evidence for this timing is given by the fact that the Calanda-phase cleavage was cataclastically reworked adjacent to the thrust plane (Schmid, 1975) (Fig. 3). We argue that this S_2 cleavage formed when the Helvetic nappes were first overridden and accreted into the Alpine wedge. The Glarus Thrust then cut back through the wedge and allowed the Helvetic nappes to move up and over a more frontal part of the Alpine wedge. As a result, the already cleaved Verrucano in the hanging wall was juxtaposed with the relatively uncleaved Infrahelvetic complex, located in the footwall.

During the last deformational event, the D_3 or Ruchi phase of Milnes and Pfiffner (1977), movement along the Glarus Thrust continued and a crenulation cleavage developed in the Infrahelvetic complex subperpendicular to the Glarus Thrust (Schmid, 1975; Milnes and Pfiffner, 1977 Lihou, 1996). The crenulation cleavage is formed within a 300-m-thick zone beneath the Glarus Thrust. This spatial association with the thrust suggests that the cleavage is somehow related to motion on the thrust (Schmid, 1975).

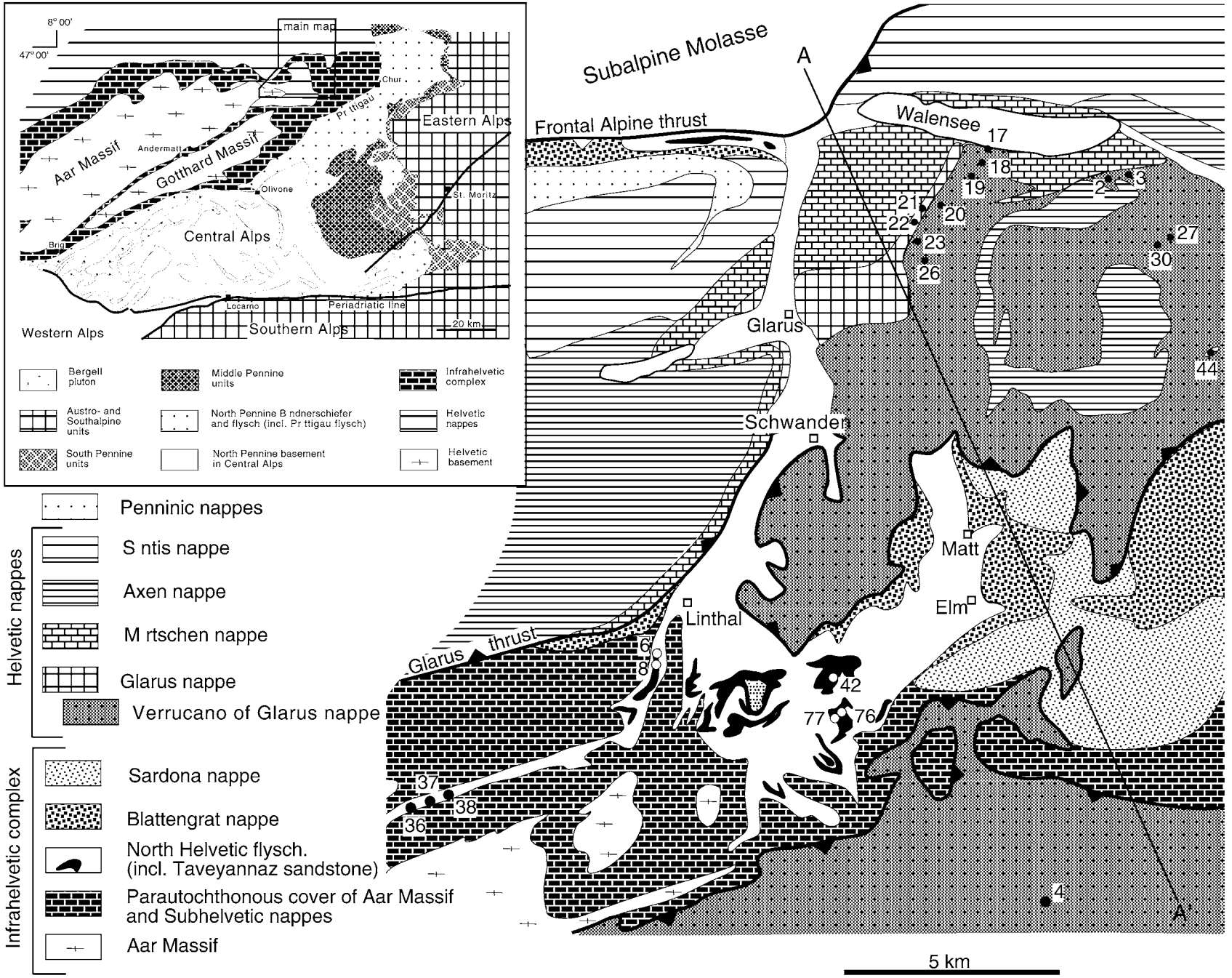

Fig. 2. Structure map of the Glarus Alps, adapted from Lihou (1996). Numbers show localities for samples reported in Table 1. The line A–A′ locates the cross-section shown in Fig. 3. The inset map shows the major tectonic zones of the Central Alps.

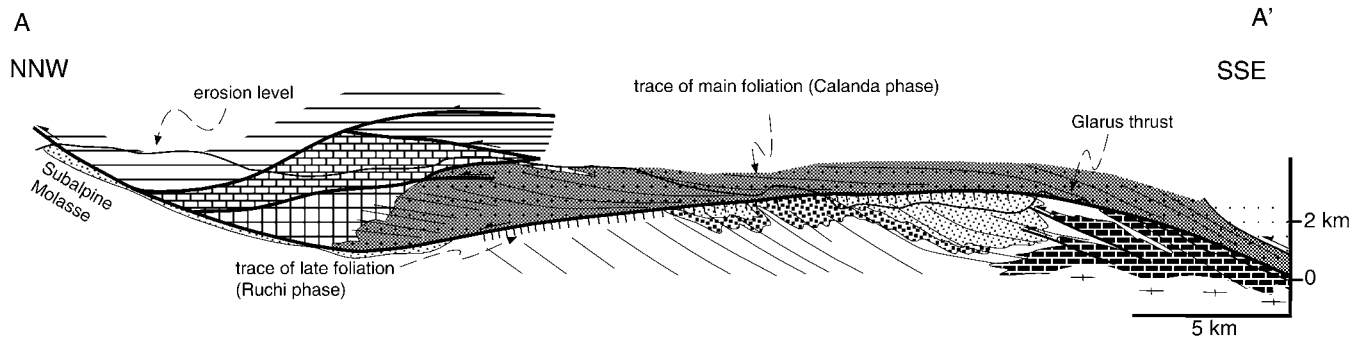

Fig. 3. Simplified cross section through Glarus Alps, modified from Schmid (1975) (see Fig. 2 for location and patterns for this section A–A′).

Subhorizontal fibres in extension gashes trend 150–160°, and are thought to track the extension direction during D_3 (Schmid, 1975).

Slip on the Glarus Thrust was, in part, post-metamorphic, resulting in an inverted metamorphic sequence, with higher grade rocks above lower grade rocks. From this, Frey (1988) concluded that about 10–20 km of the displacement along the Glarus Thrust postdated the Early Oligocene peak of metamorphism. Rahn et al. (1995) revised this estimate to about 10 km of post-metamorphic transport. K–Ar and Rb–Sr white mica dating of the Lochseiten mylonite suggests white mica growth at ~23 Ma (Hunziker et al., 1986). A later phase of slip was dated at 14–20 Ma (Frey et al., 1973). Rahn et al. (1994) showed discontinuities in apatite fission-track ages across the Glarus Thrust, providing strong evidence for a final increment of slip in the Late Miocene. The apatite fission-track study of Rahn et al. (1997) also showed late arching of the Glarus Thrust (Fig. 3) during the Late Miocene. The Middle-to-Late Miocene deformation coincides with enhanced subsidence in the Molasse basin between 17–14 Ma, followed by the deposition of conglomerate units at ~14–11 Ma (den Brok and Jagoutz, 2000).

3. Deformation study

3.1. Evidence for SMT deformation

Our strain methods are designed solely for measuring SMT deformation. In this context, we assume that all strain occurs by changes at the boundaries of grains, and that intragranular strains are negligible. We support this assumption with a detailed discussion of the deformation textures, and then follow with a description of our deformation measurement methods.

The units we sampled were dominated by siliciclastic sandstones, with quartz and feldspar occurring as the dominant detrital phases. About 30% of our sandstone samples had significant secondary carbonate. Calcite and other carbonate minerals can deform by dislocation glide at relatively low temperatures (Schmid, 1982). Thus, these samples were deemed unsuitable for our methods, and were excluded from the study. Field and thin section observations suggest no apparent difference in the ductile deformation taken up by these different types of sandstone.

In the field, the Verrucano and Melser sandstones from above the Glarus Thrust and the Tavayannaz sandstone from below the thrust showed a variably developed spaced cleavage (Fig. 4). This planar fabric was easy to see, but linear fabrics were not visible in hand samples.

Textural observations were made using thin sections cut in two principal planes, *XY* and *XZ*. (*X*, *Y* and *Z* refer to the maximum extension, intermediate and maximum shortening directions.) The *XY* section was cut parallel to cleavage, and was then used to determine the average direction of fibre overgrowths. Unidirectional fibres were observed in *XY* sections. The average fibre direction was thus considered to mark the *X* direction. *XZ* sections were cut perpendicular to cleavage and parallel to *X*. These two sections were then used to measure strain magnitudes and internal rotations.

Petrographic evidence indicates that SMT was the dominant deformation mechanism operating in the Taveyannaz sandstone samples below the Glarus Thrust. These sandstones are mainly composed of first-cycle volcanogenic sediment. Monocrystalline grains of volcanic quartz and plagioclase show little to no undulose extinction, deformation laminae, or deformation twinning. Polycrystalline quartz grains do show undulose extinction and other evidence for intracrystalline deformation. These grains are interpreted to be metamorphic detritus because the intracrystalline deformation is limited to these grains and because their microstructures lack systematic orientations. This conclusion is further supported by the fact that the metamorphic grains are commonly mantled by undeformed fibre overgrowths. The dominance of the SMT mechanism is consistent with metamorphic temperatures (see above), which were almost everywhere below the 300°C threshold needed to activate dislocation glide-and-climb in quartz (Küster and Stöckhert, 1997).

As shown by Siddans (1979), the SMT mechanism also dominates in the Verrucano above the Glarus Thrust in the northern and central Glarus Alps. The mudstones there are red and have greyish-green reduction spots, which Siddans

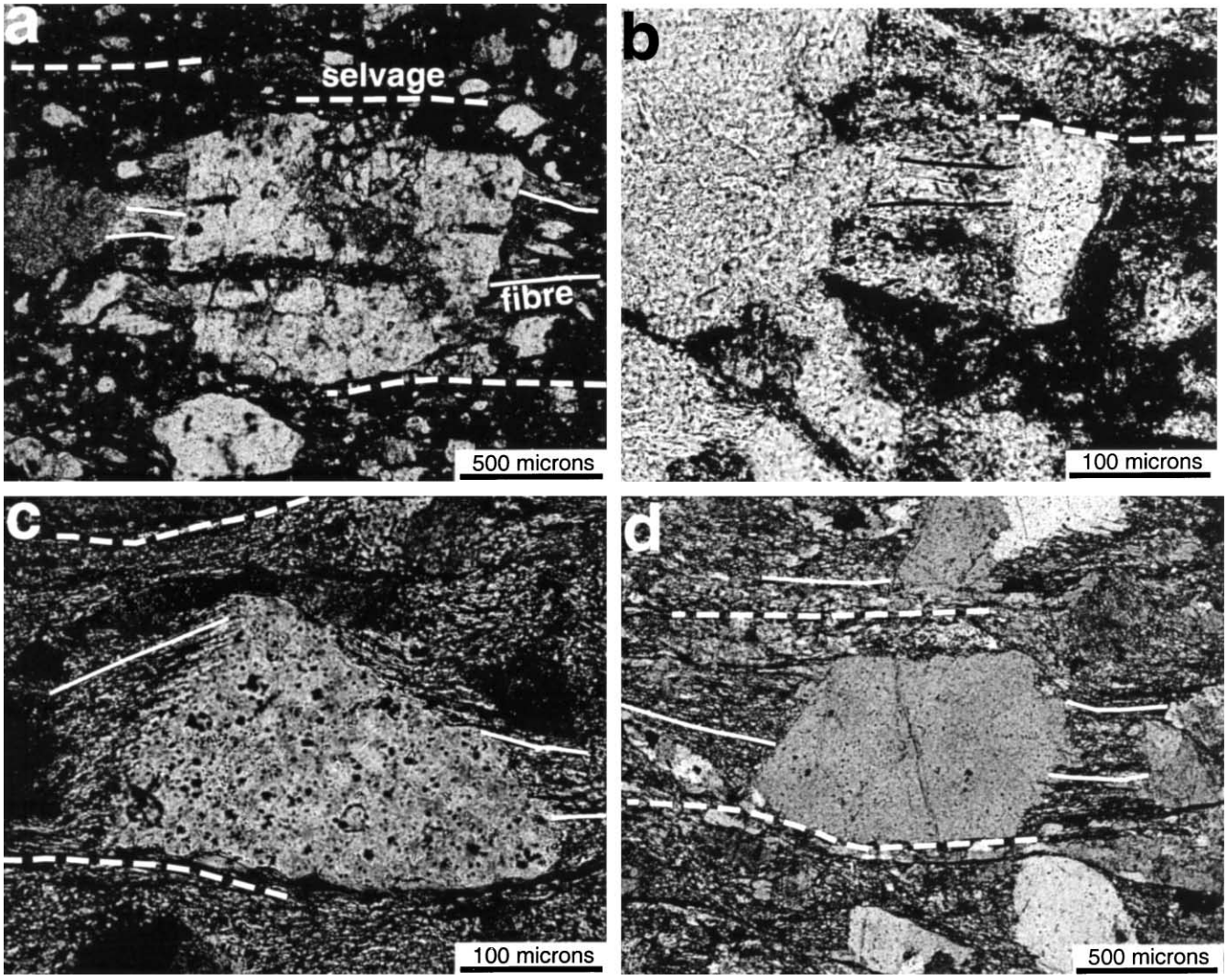

Fig. 4. Photomicrographs of SMT deformation textures. All views are *XZ* sections, with *X* in the horizontal. Dashed lines show the local trace of cleavage selvages, and solid lines mark the local trace of fibre overgrowths. (a) Feldspar clast with tapered bundles of straight fibres. The fibre bundles are, on average, parallel to selvages. This sample (#30) was determined to be nearly coaxial ($W_m^* = 0.1$). Note that the textures illustrated by this example are typical of those found in most of our samples. (b) Another example of short and straight fibres from sample #30. (c) Tapered fibre bundles on a quartz grain (sample #2). (d) Asymmetric fibre pattern around a large quartz grain (sample #4). The fibres curve slightly upward on the left, indicating heterogeneity in the local deformation. Quartz in this sample is slightly recrystallised and therefore no strain measurements have been done.

(1979) used for his strain analysis. Metamorphic grade increases to the south across the Glarus Alps. The mudstones become green, with the colour change coinciding with the development of subgrains in quartz and recrystallisation of fibre overgrowths. This transition mainly occurs to the south of the hinge of the broad arch marked by the Glarus Thrust (the hinge line runs between Linthal and Elm, Fig. 2) (see also van Daalen et al., 1999).

Quartz and feldspar are truncated by thin selvages composed of insoluble minerals. The selvages can be regarded as planes of finite flattening that formed perpendicular to *Z* (Ramsay and Huber, 1983). Directed fibrous overgrowths of quartz, chlorite, and white mica mantle those grain boundary segments at a high angle to cleavage. The fibre overgrowths are considered to record extensional strains that accumulated during SMT deformation. In *XY* and *XZ* sections, fibre bundles are typically straight and unidirectional (Fig. 4). The unidirectional geometry indicates that strains in the *Y* and *Z* directions are contractional. In contrast, some studies (e.g. Ring and Brandon, 1999) have recognised multidirectional fibres that point in all directions in the *XY* plane, indicating extension in both *X* and *Y*.

In *XZ* sections, the fibre bundles generally lie subparallel to the trace of cleavage (Fig. 4a and b). Individual fibre bundles typically have a tapered geometry, with fibres converging away from the host grain. This tapered geometry is recorded in the distribution of fibre directions, which commonly vary by as much as $\pm 15^\circ$ around the average direction.

The taper geometry has been explained as resulting from dissolution between the fibres to accommodate shortening in the *Y* and *Z* directions (semi-deformable antitaxial fibre model of Ring and Brandon, 1999). Extension parallel to *X* is accommodated solely by growth of new fibres. The fibres are inferred to accrete at the grain boundary, so that the amount of shortening across the fibres is largest at the end of the bundles. This explanation accounts for the observation that the degree of tapering seems to increase with the amount of shortening in the section. For instance, fibre bundles appear more tapered in *XZ* sections than *XY* sections because shortening is greater in *Z* than in *Y*.

We assume that the fibres track the incremental *X* direction during the deformation history of the rock, whereas cleavage records the *XY* plane for the total SMT strain. Thus, parallelism between fibres and cleavage indicates a coaxial deformation (Feehan and Brandon, 1999; Ring and Brandon, 1999). As noted above, most of our samples (80%) have fibres that parallel the trace of cleavage. However, some samples (20%) have an average fibre orientation in the *XZ* section that is oblique to the trace of cleavage (e.g. Fig. 4d), indicating a weakly non-coaxial deformation. In a few samples, we found individual fibres with an obliquity of up to 20–30° to cleavage. Nonetheless, the average angle between fibres and cleavage in these samples is less than 8°. We return to this topic below when we make specific estimates of the degree of non-coaxiality.

In some thin sections, we observed weakly curved fibre bundles around large quartz or feldspar grains (Fig. 4c and d). This texture appears to record heterogeneous deformation around the largest grains. This localised deformation is included in our measurements but tends to be averaged out at the scale of the thin section.

As discussed in Ring (1996) and Feehan and Brandon (1999), the formation of a SMT fabric requires the accommodation of small motions on the selvage surfaces to account for differential motion of adjacent grains. We see no textural evidence for throughgoing slip surfaces or for oblique shearing between grains. The deformation associated with SMT processes is accommodated solely by shortening across the selvages and extension in the fibre direction.

Textural evidence suggests that the sandstones had little porosity at the start of SMT deformation. All of the space between grains is presently occupied by selvages or directed fibre overgrowths. Dissolution along selvage surfaces would quickly remove an initial porosity. Transient porosity might have existed along the incoherent surfaces that separated the fibre overgrowths from their host grains. However, the porosity along this surface would have been small given that displacement-controlled fibre overgrowths only form when crack apertures are small, on the scale of microns or less (Urai et al., 1991; Fisher and Brantley, 1992). We can think of no other textural features that might indicate significant porosity during SMT deformation. We suggest that mechanical compaction had already removed much of the primary porosity before the onset of SMT deformation. This result would be expected for a poorly sorted sediment where grains of different sizes could be compacted into a tightly packed aggregate.

Our observations indicate that fibre overgrowth was the sole mechanism of precipitation during SMT deformation. Alternative possibilities include: (1) mass transfer associated with metamorphic recrystallisation of the original detrital grains, (2) the precipitation of syntaxial overgrowths on existing detrital grains (e.g. the overgrowth of quartz on detrital quartz grains), and (3) the formation of a fine-grained 'matrix' around the grains.

The following evidence indicates that the contribution of these other processes was minor. (1) The original grain boundaries of the detrital grains are well preserved and the grains themselves show little evidence of internal recrystallisation. (2) There is evidence of alkali mass transfer, such as albitisation of plagioclase, but this exchange appears to have occurred by in situ transfer. For instance, albitised plagioclase grains retain their detrital shapes, with no sign of recrystallisation. (3) The fibre overgrowths appear compositionally uniform within a thin section, which suggests that they grew from a common solution. In other words, they are not the product of local replacement of existing detrital grains by recrystallisation. (4) There are many descriptions in the literature of a 'fine-grained matrix' in low-grade immature sandstones. The 'matrix problem' is at the centre of the old debate about the distinction of greywacke from arkose (see Dickinson (1970) for a review). More recently, some of our colleagues have suggested that the matrix of the rock may account for the volume loss that we have measured. Deformed lithic grains can appear like matrix, but the outlines of such grains are usually easily recognised in plane light (pseudomatrix of Dickinson (1970)). Our experience is that the rest of the 'matrix' is fibre overgrowths. The overgrowths appear as a 'fine-grained matrix' when viewed in sections oblique to the *X* direction. *XY* and *XZ* sections are needed to see the overgrowth texture, with *XZ* sections providing the best view. Diagnostic features include the elongated habit of the fibre minerals (commonly quartz and mica), the consistent orientation of the fibres across the section, and the generally uniform composition of the overgrowths. (5) We found no petrographic evidence for syntaxial overgrowths, but cathodoluminscence work is needed to fully test this conclusion.

3.2. Methods

Our study employs the Projected Dimension Strain (PDS), Mode and SMT-fibre methods for measuring strains and internal rotations in sandstones deformed by the SMT mechanism. A brief summary is provided here. Further details can be found in Feehan and Brandon (1999) and Ring and Brandon (1999). Relevant computer programs are available at *www.geology.yale.edu/~brandon*.

Traditional methods, such as the R_f/ϕ method, are not suitable because the grains did not deform as passive

markers but rather by truncation and precipitation along grain boundaries. In our discussion here, the principal stretches are designated as $S_X \geq S_Y \geq S_Z$, where $S =$ final length/initial length.

Measurements were made using *XZ* and *XY* thin sections. Samples in this study have unidirectional fibres, which means that $S_X > 1$ and S_Y and $S_Z < 1$. Thus, S_Y and S_Z were determined by the PDS method, and S_X by the Mode method.

The PDS method is used to measure the average shortening produced by dissolution of grain boundaries. The method exploits the fact that for SMT deformation, the dimensions of the detrital quartz and feldspar grains remain unchanged in the *X* direction (i.e. deformation is intergranular, not intragranular). Therefore, the grain diameter in the *X* direction provides a record of the original size of the grain. The central idea behind the PDS method is that principal directions have $S < 1$, where the SMT deformation has reduced the average dimension of the detrital grains by a factor equivalent to the principal stretch. In contrast, the average initial dimension of a detrital grain should be preserved in the *X* direction because the grains lack any significant internal deformation and because the original grain surface is mantled by fibre overgrowths. Therefore, a contractive principal stretch can be determined by finding the average grain dimension parallel to a contractive principal direction and dividing it by the average grain dimension parallel to *X*. Dimensions are measured in a two-dimensional thin section, so a correction is needed to get the appropriate three-dimensional result (see Feehan and Brandon (1999) for details).

Our measurements were made using a petrographic microscope with a camera lucida tube and digitising tablet. Measurements are precise to better than ± 3 μm. The dimension of each grain is represented by its caliper dimensions (or projected dimensions) in the principal directions lying in the section. The caliper dimensions of the grains are not affected in any significant way by grain rotations associated with compaction. For instance, PDS measurements on undeformed sandstones gave undeformed results (i.e. S ~ 1) (Ring and Brandon, 1999).

The Mode method is used to determine the extensional strain recorded by the fibre overgrowths. The modal percentage of fibres in a rock is directly related to the absolute extensional stretch in the rock. Fibre modes are most easily measured in the *XZ* section. For unidirectional fibres, $S_X = (1 - m)^{-1}$, where *m* is the modal fraction of the fibre.

Given absolute strains, the volume stretch S_V (= final volume/initial volume) is equal to the product of the principal stretches ($S_X \times S_Y \times S_Z$). Because our methods focus entirely on the loss of mass from grains and the amount of mass locally precipitated, our estimates of S_V only represent the mass-transfer component of the volume strain. Other sources of volume strain include changes in porosity and mineral density. Porosity is thought to have been small at the start of SMT deformation and is thus ignored. Changes in mineral density are insignificant at the low metamorphic grade in our study area.

The geometric relationship between the fibre overgrowths and the trace of cleavage was used to estimate the internal rotation associated with SMT deformation. This method is described in Ring and Brandon (1999). The basic idea is that the fibre overgrowths track the incremental extension direction during the deformation, whereas the cleavage approximates the *XY* plane of the finite deformation. Internal rotation was estimated using the FIBRE program to model the shape of about 30–50 fibres digitised in the *XZ* section (Ring and Brandon, 1999). The internal rotation axis is assumed to parallel *Y*.

Tables 1 and 2 report internal rotation and average kinematic numbers for SMT deformation. Internal rotation is represented by a right-handed rotation axis, defined by a trend and plunge, and a rotation angle, Ω_i. W_m and W_m^* are the average kinematic vorticity numbers and A_m^* the average kinematic dilatancy number (Means et al., 1980; Passchier, 1991; Means, 1994; Ring and Brandon, 1999). Definitions and other details are given in Ring and Brandon (1999). A brief review is provided here. The *m* subscript for the kinematic numbers indicates a path-averaged value assuming a steady three-dimensional deformation. If SMT deformation were unsteady, then W_m^* would have no direct relationship to the time history of the instantaneous kinematic vorticity number W_k^*. The simple geometry of the overgrowths in our samples suggests that SMT deformation was fairly steady, at least in its orientation. An asterisk indicates that the kinematic number is based on the deviatoric stretching rate rather than the absolute stretching rate. Thus, a coaxial deformation is indicated by $W_m^* = 0$ and a non-coaxial simple-shear deformation by $W_m^* = 1$, regardless of the amount of volume strain. A_m^* describes the average ratio of the volume-strain rate relative to the deviatoric stretching rate (Passchier, 1991; Ring and Brandon, 1999). The deformation is isochoric if $A_m^* = 0$, dilatant if $A_m^* > 0$, and compactive if $A_m^* < 0$. For example, a deformation involving uniaxial shortening and an equal loss of volume, would have $A_m^* = -1$ because the rates of volume strain and deviatoric strain would be equal but opposite in sign.

Table 2 reports tensor averages for our deformation measurements. As discussed in Brandon (1995), deformation data must be averaged in tensor form to ensure that the magnitudes and directions of the principal stretches and rotations are correctly associated. If the rotational component of the deformation is small, then one can average the stretch tensor and the internal rotation tensor separately, without introducing significant errors (Brandon, 1995). In this study, tensor averages were calculated using the Hencky method where only the stretch tensor is needed (see Appendix B of Brandon (1995)).

3.3. Results

Tables 1 and 2 list our deformation measurements for the

Table 1
Measurements of SMT deformation relative to present coordinates. Notes: tr. and pl. indicates trend and plunge. Ω_i is the internal rotation angle; a positive angle indicates a right-handed rotation. Sample 4 contains recrystallised quartz grains, so principal directions were determined from R_f/ϕ measurements

No.	Stretches										Internal rotation			Kinematic numbers		
	Extension			Intermediate			Shortening			Volume						
	tr.	pl.	S_X	tr.	pl.	S_Y	tr.	pl.	S_Z	S_V	tr.	pl.	Ω_i	W_m	W_m^*	A_m^*
Above the Glarus Thrust																
Sandstones from the Verrucano Formation																
2	79	23	1.05	178	20	0.96	305	59	0.48	0.48	–	–	–	–	–	− 0.85
3	40	4	1.14	132	14	0.95	295	75	0.63	0.69	132	14	− 0.61	0.03	0.04	− 0.63
4	223	6	–	132	8	–	349	80	–	–	–	–	–	–	–	–
17	218	2	1.05	128	15	0.77	315	75	0.74	0.60	–	–	–	–	–	− 1.34
18	40	28	1.28	300	17	1.16	182	56	0.58	0.86	300	17	+ 4.05	0.18	0.18	− 0.17
19	19	4	1.06	112	42	0.75	285	48	0.65	0.52	–	–	–	–	–	− 1.31
20	201	1	1.07	291	1	0.74	21	89	0.58	0.46	–	–	–	–	–	− 1.26
23	193	7	1.33	283	1	1.02	21	83	0.63	0.85	283	1	+ 1.19	0.05	0.05	− 0.21
26	205	14	1.11	104	38	0.82	312	49	0.78	0.71	104	38	− 0.48	0.04	0.04	− 0.90
27	3	5	1.43	93	2	0.98	205	84	0.65	0.91	93	2	− 6.34	0.29	0.29	− 0.12
30	178	29	1.18	85	5	0.80	346	61	0.62	0.58	85	5	+ 1.69	0.08	0.09	− 0.83
Melser sandstone																
21	174	1	1.10	84	2	1.00	97	88	0.60	0.66	–	–	–	–	–	− 0.64
22	250	21	1.08	104	65	0.88	345	13	0.71	0.67	–	–	–	–	–	− 0.94
44	173	9	1.32	81	11	0.70	301	76	0.61	0.56	81	11	− 4.15	0.15	0.18	− 0.70
Below the Glarus Thrust																
Miscellaneous sandstones from the North Helvetic flysch																
36	342	18	1.04	82	29	0.87	224	55	0.74	0.67	–	–	–	–	–	− 1.18
37	2	8	1.05	95	18	0.85	249	70	0.59	0.53	–	–	–	–	–	− 1.10
38	312	10	1.09	51	43	0.88	212	45	0.54	0.52	–	–	–	–	–	− 0.91
Tavayannaz sandstone from the North Helvetic flysch																
6	167	13	1.06	265	32	0.81	58	55	0.70	0.60	–	–	–	–	–	− 1.21
8	102	20	1.09	203	29	1.08	342	54	0.78	0.92	–	–	–	–	–	− 0.22
42	337	12	1.03	243	19	1.01	98	67	0.65	0.68	–	–	–	–	–	− 0.75
76	173	21	1.12	79	11	0.73	323	66	0.62	0.51	–	–	–	–	–	− 1.11
77	179	36	1.10	79	14	1.05	331	51	0.64	0.74	–	–	–	–	–	− 0.50

Table 2
Regional averages for SMT deformation in present coordinates. Notes: tr. and pl. indicates trend and plunge. Ω_i is the internal rotation angle; a positive angle indicates a right-handed rotation

Stretches										Internal rotation			Kinematic numbers		
Extension			Intermediate			Shortening			Volume						
tr.	pl.	S_X	tr.	pl.	S_Y	tr.	pl.	S_z	S_V	tr.	pl.	Ω_i	W_m	W_m^*	A_m^*
Above the Glarus Thrust															
200	2	1.07	110	10	0.89	302	79	0.68	0.64	281	0	+ 2.1	0.12	0.14	− 1.08
Below the Glarus Thrust															
160	7	0.99	69	6	0.88	298	80	0.73	0.63	–	–	–	–	–	− 0.96

Verrucano and Melser sandstones from the Helvetic nappes above the Glarus Thrust, and for the Taveyannaz and North Helvetic flysch sandstones from the Infrahelvetic complex below the thrust. Sample locations are shown in Fig. 2. Note that most of our samples from the Helvetic nappes are from more than 1 km above the thrust plane.

The stereograms (Fig. 5) show that the Z directions are clustered around a steeply plunging maximum, and the X and Y directions are scattered in a weakly defined sub-horizontal girdle. The average for Z (Table 2) defines the average flattening plane, which has a strike of 30° and a dip of 10° to the SE. The average X direction is close to horizontal, although its trend changes from 200° above the Glarus Thrust to 160° below the thrust. The Nadai plot (Fig. 6) shows a scatter of both prolate and oblate strain symmetries. The strain type (Fig. 7) is generally weakly

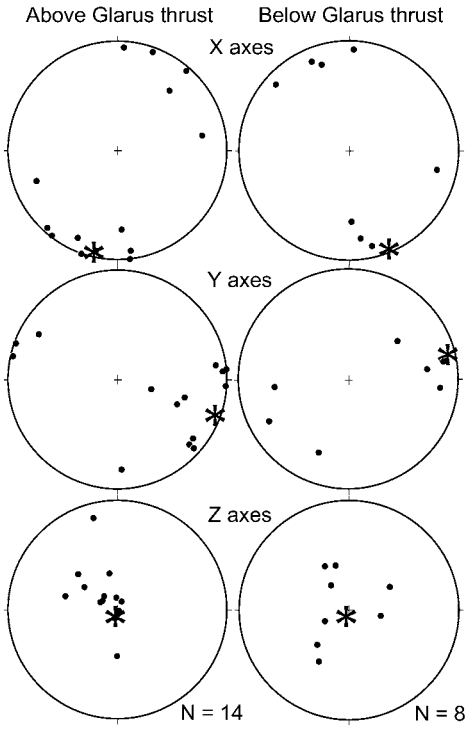

Fig. 5. Stereograms (lower-hemisphere, equal-area projection) of principal strain directions for samples above and below the Glarus Thrust (Table 1). The asterisks indicate principal directions for the tensor averages (Table 2).

constrictional, as indicated by $S_Y < 1$ (Table 1). The principal stretches indicate that the constrictional aspect of the strain is primarily the result of shortening in the Y and Z directions, and not extension in X.

Above the Glarus Thrust, local measurements from the Verrucano and Melser sandstones have X strains ranging from +5 to +43% and Z strains, from −22 to −52%. The tensor average indicates absolute principal stretches of 1.07, 0.89 and 0.68. Thus, at the regional scale, SMT deformation was constrictional ($1 > S_Y > S_Z$) and approximately plane strain ($S_X \approx 1$). This surprising result, with $S_X \approx 1$, stems from the variable orientations of X and Y in the flattening plane, which means that local extensional strains are averaged out at the regional scale.

Below the Glarus Thrust, individual samples show smaller strain magnitudes in X and Y. For instance, X strains range from +3 to +12%. In contrast, the tensor average indicates absolute principal stretches of 0.99, 0.88 and 0.73, which is nearly identical to the tensor average above the thrust. At the regional scale, sandstones above and below the fault record a similar SMT deformation involving constrictional plane strain.

The absolute strain data indicate pronounced mass-loss volume strains ranging from −9 to −54% in the sandstones above the Glarus Thrust, and −8 to −49% for sandstones below the thrust. The average is the same for both groups, −36%. At the outcrop scale, there is no evidence of where this missing mass went. The volume fraction of veins in outcrops is generally no greater than a few percent. Thus,

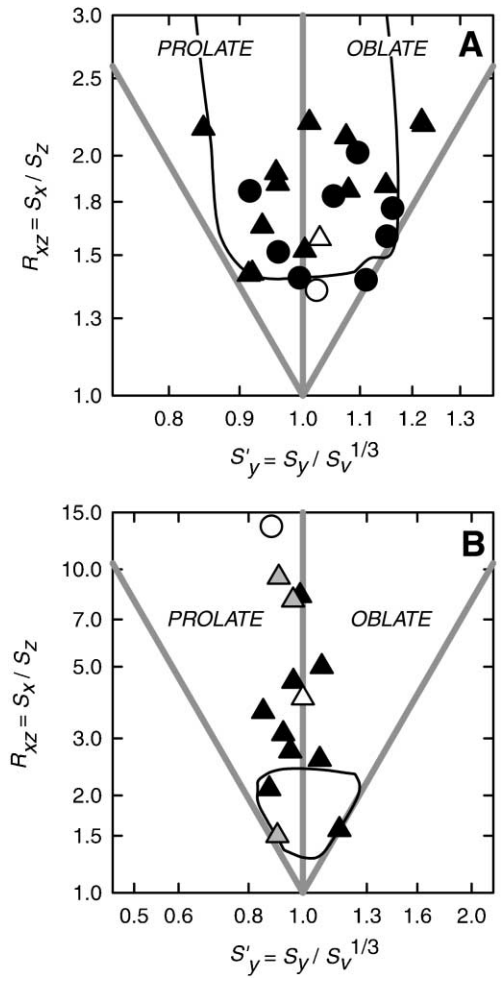

Fig. 6. Nadai plot showing strain symmetry and deviatoric strain magnitude (Brandon, 1995). S'_y is the intermediate deviatoric stretch, equal to S_y normalised to constant volume ($S'_y = S_y/S_v^{1/3}$). (a) Our measurements: circles = samples from below the Glarus Thrust, triangles = samples from above the thrust, closed symbols = individual determinations, and open symbols = tensor averages. The line outlines the lower end of the strain data distribution from Siddans (1979). (b) Previously published strain date from Siddans (1979) and Milnes and Pfiffner (1977): closed triangles (grey and black) = R_f/ϕ measurements from Siddans (1979) for reduction spots in the Verrucano mudstones, located above the Glarus Thrust. The grey triangles mark results from localities near the Glarus Thrust. Open triangle = 'average' reported by Milnes and Pfiffner (1977) for the upper plate of the Glarus Thrust (probably determined from Verrucano reduction spots); open circle = 'average' reported by Milnes and Pfiffner (1977) for highly deformed rocks directly above the Glarus Thrust. The line outlines the distribution of our measurements.

we conclude that SMT deformation was influenced by a large flux of fluid that was able to dissolve the sandstones and to transport the dissolved load over a scale larger than our study area.

Fig. 8 shows that volume strain and deviatoric strain are uncorrelated, which implies that these strains are controlled by different processes. Based on our previous work, we have found that a strong correlation between deviatoric strain and volume strain only occurs where fibre overgrowths are small or absent (e.g. Feehan and Brandon, 1999). The reason is

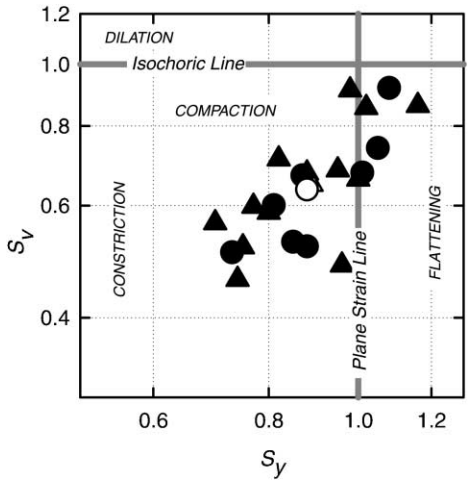

Fig. 7. Strain-type plot (Brandon, 1995) showing our absolute strain data: circles = lower plate samples, triangles = upper plate samples, closed symbols = individual determinations, and open symbols = tensor averages. The plot indicates a constrictional deformation ($S_Y < 1$) with significant compactional volume strain ($S_V < 1$).

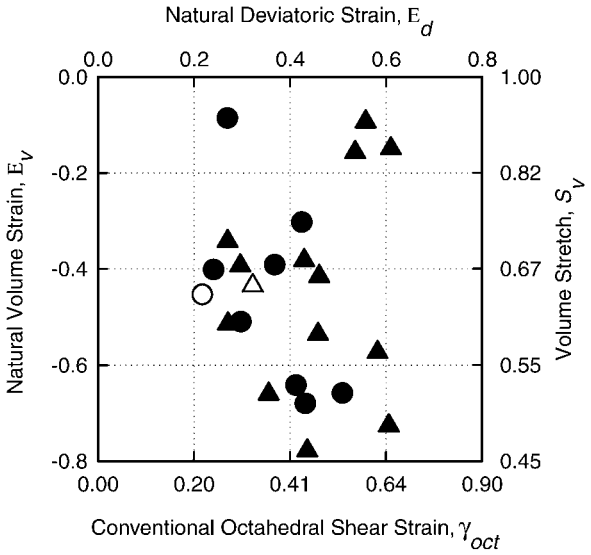

Fig. 8. The $E_v - E_d$ diagram (Brandon, 1995) is used to compare the volumetric and deviatoric components of the strain. Our strain data show no correlation, which indicates that processes responsible for volume and deviatoric components of the deformation are, at least in part, decoupled: circles = lower-plate samples, triangles = upper-plate samples, closed symbols = individual determinations, and open symbols = tensor averages. $E_v = \ln(S_v)$ and is a measure of volume strain. E_d is a measure of the average deviatoric strain, defined by $E_{d^2} = (1/3)[(E_x - E_y)^2 + (E_y - E_z)^2 + (E_x - E_z)^2]$ where E_x, E_y and E_z are the natural logarithms of the principal stretches. E_v and E_d are linearly related to the principal strain rates for a coaxial deformation. Logarithmic axes are used to show equivalent values for the volume stretch S_v and the conventional octahedral shear strain γ_{oct}. See Brandon (1995) for further details.

that volume and deviatoric strains are solely a function of shortening strains in Y and Z. Deviatoric strains become uncorrelated with volume strain when there are variations in extensional strain (as indicated by variations in the modal abundance of fibre overgrowths). Uncorrelated volume strain and deviatoric strain are observed in the Eastern Belt of the Franciscan Complex of California (Ring and Brandon, 1999), as well as in our Glarus study here. The variations in fibre overgrowths means that some of the dissolved grain mass is re-precipitated locally in the rock. The rock must extend in at least one direction to be able to accommodate the locally precipitated mass.

Only seven out of the 18 samples have sufficient extensional strain to determine the rotational component of the deformation, Ω_i and W_m^* (Table 1). Small extensional strains means short fibres. As the fibres get shorter, so does the resolution of the incremental extension path. S_X must be greater than ~1.10 to get reliable estimates of Ω_i and W_m^* (Ring and Brandon, 1999). Our measurements indicate minor non-coaxiality during SMT deformation. One sample has $W_m^* = 0.29$, but the rest are less than 0.18. The rotational component of the deformation may be relatively small, but the internal rotation axes show a consistent orientation and shear sense (Fig. 9). The average rotation axis (Table 2, asterisk in Fig. 9) is horizontal and indicates a general top-north sense of shear, which is similar to the shear-sense direction determined for the Glarus Thrust (Schmid, 1975; Milnes and Pfiffner, 1980; Lihou, 1996).

3.4. Previous regional strain work

Siddans (1979) presents principal strain ratios measured from reduction spots in mudstones at 12 localities in the Verrucano Formation. Milnes and Pfiffner (1977) report some 'average' strain ratios for areas adjacent to the Glarus Thrust, but the details of their measurements and the localities are not discussed. Neither study provides any information about principal directions. By themselves, strain-ratio data have limited utility, but they do provide information about the symmetry and magnitude of the deviatoric component of the strain. Thus, comparisons with our data are limited to the Nadai plot (Fig. 6).

All data sets show a similar clustering along the prolate/oblate boundary, so they share the same strain symmetry. In contrast, they have very different strain magnitudes. In Fig. 6, the strain ratio R_{XZ} ($= S_X/S_Z$) provides a useful measure of deviatoric strain magnitude (note that R_{XZ} is independent of volume strain). Our measurements have R_{XZ} ranging from 1.4 to 2.3, whereas Siddans' (1979) measurements range from 1.5 to 9.5. However, the highest strain magnitudes for Siddans' data are those from localities near the Glarus Thrust (grey triangles in Fig. 6b). The remaining localities (black triangles in Fig. 6b) show a closer correspondence to our results. The 'averages' given in Milnes and Pfiffner (1977) have an R_{XZ} of ~4 for rocks below the Glarus Thrust (open triangle in Fig. 6b) and ~13 for rocks directly above the thrust (open circle in Fig. 6b).

These results suggest that differences between these studies are due, at least in part, to differences in sample coverage of a heterogeneous strain field, with the heterogeneity influenced, at least in part, by the proximity to the

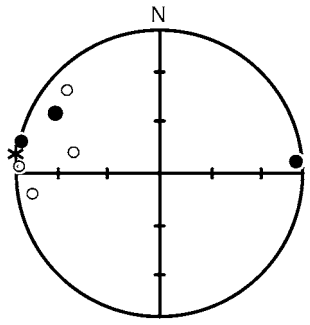

Fig. 9. Equal-area stereogram showing internal-rotation axes determined for samples from above the Glarus Thrust (Table 1). Points are right-handed rotation vectors, with closed and open symbols indicating lower and upper hemisphere directions, respectively. Six out of the seven measurements indicate a consistent top-north shear sense. The asterisk shows the mean direction for the internal-rotation axes (Table 2), which also shows a top-north shear sense.

Glarus Thrust. A denser and more uniform coverage would be needed to test this interpretation. Grain-size effects might also be important. Our study focused exclusively on medium-grain sandstones, whereas Siddans' (1979) study was restricted to Verrucano mudstones, where the reduction spots are found. Milnes and Pfiffner (1977) did not report what they sampled, but we suspect that they also focused on the Verrucano mudstones because of the availability of reduction spots.

4. Discussion

4.1. Mass loss

A surprising result of our study is the large mass loss, about 36%, in sandstones above and below the Glarus Thrust. The amount of dissolved mass is large, and there is no obvious repository for this dissolved mass in the region around the Glarus Thrust. The volume strain can be considered as a form of internal erosion within the Alpine wedge. SMT deformation included both closed and open exchange, involving local precipitation of fibre overgrowths and wholesale loss of mass from the rock. The open-system behaviour was probably driven by dissolution and bulk removal of the more soluble components of the rock, due to flow of a solvent fluid phase on a regional scale. Burkhard et al. (1992) argues for advection of externally derived fluids, associated with large fluid-to-rock ratios, during motion of the Helvetic thrust. Carbonate-bearing veins in the Taveyannaz sandstone, which is otherwise free of carbonate, also indicate mass transfer over distances greater than the outcrop scale.

Our results here are similar to those from other studies we have done on sandstones in convergent wedge settings. These include the Late Cretaceous San Juan–Cascade nappes (Feehan and Brandon, 1999), the Late Cenozoic Olympic subduction complex (Brandon and Kang, 1995), the Mesozoic Franciscan subduction complex (Ring and Brandon, 1999; Bolhar and Ring, 2001), and the Permian–Cretaceous Torlesse subduction complex in the South Island of New Zealand (Maxelon et al., 1998). All examples show significant mass loss in association with an approximately plane-strain coaxial deformation at the regional scale.

Our study highlights an interesting contrast in the character of mass transfer with increasing grade. The mass loss that we have documented in the low-grade sandstones tends to be pervasive throughout the rock. In contrast, mass transfer in greenschist- and amphibolite-facies rocks tends to be more localised, occurring in association with veins and ductile shear zones (e.g. Selverstone et al., 1991; Newman and Mitra, 1993; Ague, 1994; Bailey et al., 1994; O'Hara, 1994; Ring, 1999).

There has been recurring evidence that SMT deformation is commonly associated with large mass-loss volume strains (e.g. Wright and Platt, 1982; Wright and Henderson, 1992). This result, however, has been difficult to reconcile with the fact that silicate minerals have very low solubilities in typical metamorphic fluids. Thus, large mass-loss volume strains seem to require large fluid-to-rock ratios. One way out of this dilemma, proposed by Etheridge (1983), is that fluid flow in low-grade settings is driven by thermal convection, which would allow re-circulation of a small volume of fluid. This interpretation is supported by theoretical models discussed by Wood and Hewitt (1982, 1984) and Criss and Hoffmeister (1991), which show that there is no threshold for the onset of thermal convection when isotherms are inclined. Convection will always occur, although the flow velocities may become quite small if the thermal gradients are small. We speculate that porous-medium convective flow may be an under-appreciated process in convergent wedges, despite the low temperatures and low permeabilities thought to typify this setting.

4.2. Regional tectonic evolution

There is evidence in the Helvetic Alps that deformation propagated northward with time, starting in the structurally highest and most internal units to the south (Sardona and Blattengrat nappes) and moving outward to more external and structurally deep units to the north. Lihou (1996) related cleavage formation in the Sardona and Blattengrat nappes to the Late Eocene D_1 Pizol phase and reported a gently plunging ~160°-trending extension direction. We concur with Milnes and Pfiffner (1977) that the Glarus Thrust formed during the subsequent D_2 Calanda phase and accommodated early transport of the Helvetic nappes onto the Infrahelvetic complex. Cleavage in the Verrucano is thought to have formed early during the Calanda phase. The average X direction for the Verrucano was gently plunging with a ~200° trend at that time (Siddans, 1979; this study). We tie cleavage formation in the Taveyannaz sandstone and the North Helvetic Flysch to the late Calanda phase and the D_3 Ruchi phase (Schmid, 1975). The average X tend was

~160° at that time, identical to that reported by Schmid (1975) for the D_3 Ruchi phase. Therefore, we suggest that the Taveyannaz sandstone and the associated North Helvetic flysch, which lie beneath the Glarus Thrust, were deformed after the Verrucano and Melser sandstone, which lie above the thrust.

Overall, the data suggest that the downward propagation of deformation during the Oligocene Calanda and Ruchi phases was associated with a curving *X* direction that changed from ~200 to ~160°. However, the problem with interpreting this changing *X* direction is that our strain work indicates that little extension was associated with *X* above and below the Glarus Thrust. In other words, the regional-scale constrictional plane-strain deformation associated with D_2 and D_3 was produced by shortening in the *Y* and *Z* directions. We also note the interpretation of *X* as a direction of tectonic transport is only valid for a simple-shear deformation, which is not supported by our strain data. The observation that the SMT strains are, in general, only slightly non-coaxial also challenges the interpretation that the ductile deformation in the nappe is related to shear coupling on the Glarus Thrust. In contrast, we argue that the generally coaxial deformation away from the Glarus Thrust indicates that the thrust was very weak. In fact, experimental work by Hsü (1969) and Schmid (1975) showed that the Lochseitenkalk is very weak. Likewise, very low shear coupling on subduction thrusts has been proposed by Brandon and Ring (1998), who summarised five quantitative studies of ductile deformation from deeply exhumed accretionary wedges. They concluded that flow there is almost always coaxial because the subduction thrust was too weak to transmit a significant shear traction.

These findings bring up the question of how intra-nappe deformation relates to nappe translation in orogens. In general, there are two different ideas in thrust belts. The first is that ductile strain in nappes is distinctly non-coaxial with stretching lineations parallel to thrust transport at the base of the nappes. A certain amount of coupling at faults is needed to internally shear adjacent thrust nappes. In the western Helvetic nappes for example, the carbonates of the Morcles nappe shows strong evidence for non-coaxial shear (Ramsay and Huber, 1983). Studies in the strongly ductilely deformed Penninic nappes also appear to support such a view (e.g. Merle et al., 1989; Ring, 1992). The second idea is that faults are weak, as suggested for the Lochseitenkalk at the Glarus Thrust (Hsü, 1969; Schmid, 1975). The two different concepts may, at least in part, depend on the strength contrast between the mylonite between nappes and the interior of the nappe. The viscosities of the carbonates of the Morcles nappe and the Lochseitenkalk are different. In the Morcles nappe, limestones are deformed by dislocation creep (Ramsay and Huber, 1983). For the Lochseiten mylonite, Schmid (1982) proposed deformation by superplastic flow. We have shown that deformation in the Glarus nappe and the North Helvetic flysch is approximately coaxial, as expected for a weak thrust. Therefore, the Lochseitenkalk was probably considerably weaker than the limestone in the Morcles nappe and this rheologic contrast might have controlled the different structural styles in the Helvetic nappes of western and eastern Switzerland.

We propose that deep accretion (i.e. underplating) caused vertical thinning of the overlying wedge, as recorded by the formation of a subhorizontal cleavage in the hanging wall of the Glarus Thrust. Vertical shortening of 30% appears to be balanced by mass loss. Our rotation data show that the foliation formed during a weakly non-coaxial deformation within large parts of the Glarus nappe. In a typical foreland fold-and-thrust belt, one would expect the foliation in a thrust sheet to be at a high angle to the underlying thrust and then curving asymptotically into subparallelism with the thrust plane. Theoretically, the flat-lying foliation in the Verrucano could be due to rotation as a result of large non-coaxial strains, i.e. that the Verrucano represents a huge shear zone at the base of the Helvetic nappes. We regard this option as unrealistic because of the regionally low strains and the lack of evidence for pronounced non-coaxial deformation in large parts of the Verrucano. We propose that the flat-lying foliation in the Verrucano is basically a result of pronounced vertical shortening that accompanied nappe translation. This would imply that early Calanda-phase nappe stacking in the Glarus Alps was not by simple shear. It also implies that the exhumation of the Glarus Thrust was not solely due to erosion but has also been aided by coaxial vertical shortening. Assuming an initial depth of 12–15 km and a residence time within the ductile crust of about 25 My, we calculate, using the one-dimensional numerical model of Feehan and Brandon (1999), that ductile thinning contributed ~1.5 km (~10%) to the exhumation of the Glarus Thrust.

Acknowledgements

This study was funded by the Deutsche Forschungsgemeinschaft through the Graduiertenkolleg "Stoffbestand von Kruste und Mantel" at Mainz University and a US/German exchange program funded by the National Science Foundation (NSF INT-9513911) and the Deutscher Akademischer Austauschdienst. Brandon acknowledges additional NSF support from EAR 9814807. We thank Meinert Rahn, Bas den Brok and Oliver Jagoutz for numerous discussions and Stefan Schmid and Kyuichi Kanagawa for careful reviews and Richard Lisle for editorial handling.

References

Ague, J., 1994. Mass transfer during Barrovian metamorphism of pelites, south-central Connecticut, I: evidence for composition and volume change. American Journal of Science 294, 989–1057.

Bailey, C.M., Simpson, C., de Paor, D.G., 1994. Volume loss and tectonic

flattening in granitic mylonites from the Blue Ridge province, central Appalachians. Journal of Structural Geology 16, 1403–1416.

Bertrand, M., 1884. Rapport de structure des Alpes de Glaris et du bassin houiller du Nord. Bulletin Geoloquie de France 3 (12), 318–330.

Bolhar, R., Ring, U., 2001. Deformation history of the Yolla Bolly terrane at Leech Lake Mountain, Eastern belt, Franciscan Subduction Complex, California Coast Ranges. Geological Society of America Bulletin 113, 181–195.

Brandon, M.T., 1995. Analysis of geologic strain data in strain-magnitude space. Journal of Structural Geology 17, 1375–1385.

Brandon, M.T., Kang, B., 1995. Exhumation processes operating above the Cascadia subduction zone, NW Washington State. Terra Nova 7, 170.

Brandon, M.T., Ring, U., 1998. Viscous flow and exhumation in Franciscan-like wedges. Geological Society of America Abstracts with Programs 31 (6), 40.

den Brok, B., Jagoutz, O., 2000. The Glarus Thrust as an erosional unconformity? An old idea of Otto Ampferer revisited. 17th Swiss Tectonic Studies Group Meeting, p. 27.

Burkhard, M., Kerrich, R., Maas, R., Fyfe, W.S., 1992. Stable and Sr-isotope evidence for fluid advection during thrusting of the Glarus nappe (Swiss Alps). Contributions to Mineralogy and Petrology 112, 293–311.

Criss, R., Hoffmeister, A., 1991. Application of fluid dynamics principles in tilted permeable media to terrestrial hydrothermal systems. Geophysical Research Letters 18, 199–202.

Dickinson, W., 1970. Interpreting detrital modes of graywacke and arkose. Journal of Sedimentary Petrology 40, 695–707.

Elliott, D., 1973. Diffusion flow laws in metamorphic rocks. Geological Society of America Bulletin 84, 2645–2664.

Etheridge, M.A., 1983. Differential stress magnitudes during regional deformation and metamorphism: upper bound imposed by tensile fracturing. Geology 11, 231–234.

Feehan, J.G., Brandon, M.T., 1999. Contribution of ductile flow to exhumation of low *T*–high *P* metamorphic rocks: San Juan–Cascade Nappes, NW Washington State. Journal of Geophysical Research B104, 10883–10901.

Fisher, D.M., Brantley, S.L., 1992. Models of quartz overgrowth and vein formation: deformation and episodic fluid flow in an ancient subduction zone. Journal of Geophysical Research 97, 20043–20061.

Frey, M., 1988. Discontinuous inverse metamorphic zonation, Glarus Alps, Switzerland: evidence from illite "crystallinity" data. Schweizerische Mineralogische Petrographische Mitteilungen 68, 171–183.

Frey, M., Hunziker, J.C., Roggwiler, P., Schindler, C., 1973. Progressive niedriggradige Metamorphose glaukonitführender Horizonte in den helvetischen Alpen der Ostschweiz. Contributions to Mineralogy and Petrology 39, 185–218.

Frey, M., Hunziker, J.C., Frank, W., Bocquet, J., Dal Piaz, G.V., Jäger, E., Niggli, E., 1974. Alpine metamorphism of the Alps—a review. Schweizerische Mineralogische Petrographische Mitteilungen 54, 247–290.

Greene, M., 1982. Geology in the Nineteenth Century. Cornell University Press, Ithaca 324pp.

Heim, A., 1919. Geologie der Schweiz 2: Die Schweizer Alpen. Tauchnitz, Leipzig.

Hsü, K.J., 1969. A preliminary analysis of the statics and kinematics of the Glarus overthrust. Eclogae Geologicae Helvetiae 62, 143–154.

Hunziker, J.C., Frey, M., Clauer, N., Dallmeyer, R.D., Friedrichsen, H., Flehming, W., Hochstrasser, K., Roggwiller, P., Schwandner, H., 1986. The evolution of illite to muscovite: mineralogical and isotopic data from the Glarus Alps, Switzerland. Contributions to Mineralogy and Petrology 92, 157–180.

Küster, M., Stöckhert, B., 1997. Density changes of fluid inclusions in high-pressure/low-temperature metamorphic rocks from Crete: a thermobarometric approach to the creep strength of host minerals. Lithos 41, 151–167.

Lihou, J.C., 1996. Structure and deformational history of the Infrahelvetic flysch units, Glarus Alps, eastern Switzerland. Eclogae Geologicae Helvetiae 89, 439–460.

Maxelon, M., Wohlers, A., Halama, R., Ring, U., Mortimer, N., Brandon, M.T., 1998. Ductile strain in the Torlesse Wedge, South Island, New Zealand. EOS 79 (45), 889.

Means, W.D., 1994. Rotational quantities in homogeneous flow and the development of small-scale structure. Journal of Structural Geology 16, 437–445.

Means, W.D., Hobbs, B.E., Lister, G.S., Williams, P.F., 1980. Vorticity and non-coaxiality in progressive deformation. Journal of Structural Geology 5, 279–286.

Merle, O., Cobbold, P.R., Schmid, S.M., 1989. Tertiary kinematics in the Lepontine dome. Geological Society of London Special Publications 45, 113–134.

Milnes, A.G., Pfiffner, O.A., 1977. Structural development of the Infrahelvetic complex, eastern Switzerland. Eclogae Geologicae Helvetiae 70, 83–95.

Milnes, A.G., Pfiffner, O.A., 1980. Tectonic evolution of the Central Alps in the cross section St. Gallen-Como. Eclogae Geologicae Helvetiae 73, 619–633.

Mullis, A., 1993. Determination of the rate-limiting mechanism for quartz pressure solution. Geochemica Cosmochemica Acta 57, 1499–1503.

Newman, J., Mitra, G., 1993. Lateral variations in mylonite zone thickness as influenced by fluid-rock interactions, Linville Falls fault, North Carolina. Journal of Structural Geology 15, 849–863.

O'Hara, K.D., 1994. Fluid-rock interaction in crustal shear zones: a directed percolation approach. Geology 22, 843–846.

Passchier, C.W., 1991. The classification of dilatant flow types. Journal of Structural Geology 13, 101–104.

Paterson, M.S., 1995. A theory for granular flow accommodated by material transfer via an intergranular fluid. Tectonophysics 245, 135–151.

Pfiffner, O.A., 1978. Der Decken- und Kleinfaltenbau im Infrahelvetikum der Ostschweiz. Eclogae Geologicae Helvetiae 71, 61–84.

Pfiffner, O.A., 1981. Fold and thrust tectonics in the Helvetics nappes (East Switzerland). In: McClay, K.R., Price, N.J. (Eds.). Thrust and Nappe Tectonics. Geological Society of London Special Publication 9, pp. 319–327.

Pfiffner, O.A., 1986. Evolution of the north Alpine foreland basin in the Central Alps. In: Allen, P.A., Howewood, P. (Eds.). Foreland Basins. International Association of Sedimentologists Special Publication 8, pp. 219–228.

Rahn, M., Mullis, J., Edelbrock, K., Frey, M., 1994. Very low grade metamorphism of the Taveyannaz greywacke, Glarus Alps, Switzerland. Journal of Metamorphic Geology 12, 625–641.

Rahn, M., Mullis, J., Edelbrock, K., Frey, M., 1995. Alpine metamorphism in the North Helvetic flysch of the Glarus Alps, Switzerland. Eclogae Geologicae Helvetiae 88, 157–178.

Rahn, M., Hurford, A.J., Frey, M., 1997. Rotation and exhumation of a thrust plane: Apatite fission—track data from the Glarus Thrust, Switzerland. Geology 25, 599–602.

Raj, R., Chyung, C., 1981. Solution-precipitation creep in glass ceramics. Acta Metallurgica 29, 159–166.

Ramsay, J.G., Wood, D.S., 1973. The geometric effects of volume change during deformation processes. Tectonophysics 16, 263–277.

Ramsay, J.G., Huber, M.I., 1983. The Techniques of Modern Structural Geology, Volume 1: Strain Analysis. Academic Press, London, UK 307pp.

Ring, U., 1992. An Alpine kinematical analysis of the Penninic nappes east of the Lepontine dome: implications for the evolution of the Central Alps. Tectonics 11, 1139–1158.

Ring, U. 1996. Kinematic analysis of heterogeneous brittle deformation at the Coast Range fault zone and ductile strain and mass loss in the Eastern Franciscan belt (Franciscan subduction complex, USA): implications for the exhumation of high-pressure/low-temperature metamorphic rocks. Unpublished Habilitation thesis, Universität Mainz, 164pp.

Ring, U., 1999. Volume loss, fluid flow and coaxial vs noncoaxial deformation in retrograde, amphibolite-facies shear zones, northern Malawi,

east-central Africa. Geological Society of America Bulletin 111, 123–142.

Ring, U., Brandon, M.T., 1999. Ductile deformation and mass loss in the Franciscan subduction complex: implications for exhumation processes in accretionary wedges. In: Ring, U., Brandon, M.T., Lister, G.S., Willett, S.D. (Eds.). Exhumation Processes: Normal Faulting, Ductile Flow and Erosion. Geological Society of London Special Publication 154, pp. 55–86.

Rutter, E.H., 1983. Pressure solution in nature, theory and experiment. Journal Geological Society of London 140, 725–740.

Schmid, S.M., 1975. The Glarus overthrust: Field evidence and mechanical model. Eclogae Geologicae Helvetiae 68, 247–280.

Schmid, S.M., 1982. Microfabric studies as indicators of deformation mechanisms and flow laws operative in mountain building. In: Hsü, K. (Ed.). Mountain Building Processes. Academic Press, London, pp. 95–115.

Selverstone, J., Morteani, G., Staude, J.-M., 1991. Fluid channelling during ductile shearing: transformation of granodiorite into aluminous schist in the Tauern Window, Eastern Alps. Journal of Metamorphic Geology 9, 419–431.

Siddans, A.W.B., 1979. Deformation, metamorphism and texture development in Permian mudstones of the Glarus Alps (Eastern Switzerland). Eclogae Geologicae Helvetiae 72, 601–621.

Sinclair, H.D., 1992. Turbidite sedimentation during Alpine thrusting: The Taveyannaz sandstones from eastern Switzerland. Sedimentology 39, 837–856.

Suess, E., 1904. Sur la nature des charriages. C.R. Acad. Sci. Paris 139, 714–716.

Suess, E., 1909. Das Antlitz der Erde, III. Band, 2. Teil. Tempsky, Wien 789pp.

Trümpy, R., 1969. Die helvetischen Decken der Ostschweiz: Versuch einer palinspastischen Korrelation und Ansätze zu einer kinematischen Analyse. Eclogae Geologicae Helvetiae 62, 105–142.

Trümpy, R., 1980. Geology of Switzerland: A Guide Book. Part A: An Outline of the Geology of Switzerland. Wepf & Co., Basel.

Trümpy, R., 1998. Tectonic units of central Switzerland: their interpretation from A.D. 1708 to the present day. Bulletin Angewandte Geologie 3, 163–182.

Urai, J., Williams, P.F., van Roermund, H., 1991. Kinematics of crystal growth in syntectonic fibrous veins. Journal of Structural Geology 13, 823–836.

van Daalen, M., Heilbronner, R., Kunze, K., 1999. Orientation anaylsis of localized shear deformation in quartz fibres at the brittle-ductile transition. Tectonophysics 303, 83–108.

Wood, J.R., Hewitt, T.A., 1982. Fluid convection and mass transfer in porous sandstone—a theoretical approach. Geochemica Cosmochemica Acta 46, 1707–1713.

Wood, J., Hewitt, T., 1984. Reservoir diagenesis and convective fluid flow. In: McDonald, D., Surdam, R. (Eds.). Clastic Diagensis. American Association of Petroleum Geologists, Memoir 37, pp. 99–110

Wright, T.O., Platt, L.P., 1982. Pressure dissolution and cleavage in the Martinsburg shale. American Journal of Science 282, 122–135.

Wright, T.O., Henderson, J.R., 1992. Volume loss during cleavage formation in the Meguma Group, Nova Scotia, Canada. Journal of Structural Geology 14, 281–290.